Original Paper

Kyoji Sassa · Osamu Nagai · Renato Solidum · Yoichi Yamazaki · Hidemasa Ohta

An integrated model simulating the initiation and motion of earthquake and rain induced rapid landslides and its application to the 2006 Leyte landslide

Abstract A gigantic rapid landslide claiming over 1,000 fatalities was triggered by rainfalls and a small nearby earthquake in the Leyte Island, Philippines in 2006. The disaster presented the necessity of a new modeling technology for disaster risk preparedness which simulates initiation and motion. This paper presents a new computer simulation integrating the initiation process triggered by rainfalls and/or earthquakes and the development process to a rapid motion due to strength reduction and the entrainment of deposits in the runout path. This simulation model *LS-RAPID* was developed from the geotechnical model for the motion of landslides (Sassa 1988) and its improved simulation model (Sassa et al. 2004b) and new knowledge obtained from a new dynamic loading ring shear apparatus (Sassa et al. 2004a). The examination of performance of each process in a simple imaginary slope addressed that the simulation model well simulated the process of progressive failure, and development to a rapid landslide. The initiation process was compared to conventional limit equilibrium stability analyses by changing pore pressure ratio. The simulation model started to move in a smaller pore pressure ratio than the limit equilibrium stability analyses because of progressive failure. However, when a larger shear deformation is set as the threshold for the start of strength reduction, the onset of landslide motion by the simulation agrees with the cases where the factor of safety estimated by the limit equilibrium stability analyses equals to a unity. The field investigation and the undrained dynamic loading ring shear tests on the 2006 Leyte landslide suggested that this landslide was triggered by the combined effect of pore water pressure due to rains and a very small earthquake. The application of this simulation model could well reproduce the initiation and the rapid long runout motion of the Leyte landslide.

Keywords Leyte landslides · Computer simulation · Rapid landslides · Ring shear test

Introduction

Rapid landslides cause big disasters such as the Hattian Balla landslide triggered by the 2004 Kashmir, Pakistan, the 2006 Leyte landslide triggered by a small nearby earthquake after a heavy rainfall in the Philippines, and many big landslides triggered by the 2008 Wenchuan earthquake in Sichuan, China which have claimed over 1,000 fatalities. One of the global issues in the field of landslides, the Usoy landslide and its resulted landslide dam "Sarez Lake". The landslide of 1.1 billion m³ in volume was triggered by an earthquake in 1911 (estimated as Magnitude 7.4, Stone 2009) and it created a landslide 567 m high dam. The water level of the landslide dam has gradually increased until 38 m below the dam crest. The development of a reliable and practical landslide risk assessment technology focusing its initiation, and the resulting hazard area is currently needed. Rapid landslides causing big disasters are often triggered by earthquakes or the

combined effects of earthquakes and rains. The computer simulation incorporating the initiation process of landslides triggered by earthquakes and rains in addition to the runout is required for the disaster preparedness.

A special lecture "Geotechnical model for the motion of landslides" in the fifth International Symposium on Landslides (Sassa 1988) was to simulate the Ontake landslide triggered by the 1984 Naganoken–Seibu Earthquake. The landslide mass of 36 million m³ traveled more than 10 km along torrents. The dynamics why such a rapid and long runout motion occurred was interesting topics in interdisciplinary fields of scientists. The paper explained the low apparent friction angle estimated from the geotechnical tests and a new computer simulation incorporating the apparent friction angle mobilized during motion controlling mobility, and also the lateral pressure ratio representing the softness of landslide mass.

The apparent friction angle mobilized during rapid shearing could not be directly measured at that time. The development of the undrained dynamic-loading ring-shear apparatus (Sassa et al. 2004a) enabled to measure the apparent friction angle from the initiation to the motion within laboratory. The knowledge of apparent friction angle during motion increased by various experiments using this apparatus. The geotechnical model for the motion of landslides in 1988 was improved as a simulation model in the expression of three-dimensional view of motion through the IPL M-101 Areal prediction of earthquake and rain induced rapid traveling flow phenomena (APERITIF project) (Sassa et al. 2004b). Undrained ring shear tests presented that the undrained steady-state strength is almost same, independent of initial loaded normal stress in soils of crushable grains, because pore pressure generation continues until the effective stress reaches a critical stress under which no further grain crushing and volume reduction occur (Okada et al. 2000). Using this relation, the apparent friction coefficient is calculated from the depth of soil mass and the steady state during motion. Then, the variable apparent friction coefficient was incorporated (Wang and Sassa 2007).

A thematic session on "Benchmarking exercise on landslide debris runout and mobility modeling" was organized in the 2007 International Forum on Landslide Disaster Management in Hong Kong, China (Review by Hungr et al. 2007b). Thirteen team participated from Austria, Canada, China, France, Netherlands, Italy, Japan, Norway, Spain, and USA, and 17 models including Sassa and Wang, DAN3D (Hungr et al. 2007a; Hungr 2009), MADFlow (Chen and Lee 2003, 2007). In addition to those 17 models presented in the Forum, Denlinger and Iverson (2004), Takahashi and Tsujimoto (2000), and others conducted computer simulation for the motion of debris flows and avalanches.

All models are calibration-based, meaning that the appropriate rheological parameters cannot be determined from laboratory tests, but must be constrained by trial-and-error back-analysis of known real landslides. One characteristics of

the presented model *(LS-RAPID)* is to try to conduct it based on laboratory testing and monitored seismic records when available though it is hard task and it is not still complete.

All mentioned models aim to do *dynamic analysis* for the motion of landslides and debris flows. The initiation process is the target of *stability analysis* such as the limit equilibrium analyses, FEM analysis. Stability is out of scope of dynamic analysis. Another characteristics of *LS-RAPID* aims to integrate the initiation process (*stability analysis*) by pore pressure increase and seismic loading, and the moving process (*dynamic analysis*) including the process of volume enlargement by entraining unstable deposits within the traveling course.

Basic principle of simulation

The basic concept of this simulation is explained using Fig. 1. A vertical imaginary column is considered within a moving landslide mass. The forces acting on the column are (1) self-weight of column (*W*), (2) Seismic forces (vertical seismic force *Fv*, horizontal *x–y* direction seismic forces *Fx* and *Fy*), (3) lateral pressure acting on the side walls (*P*), (4) shear resistance acting on the bottom (*R*), (5) the normal stress acting on the bottom (*N*) given from the stable ground as a reaction of normal component of the self-weight, (6) pore pressure acting on the bottom (*U*).

The landslide mass (m) will be accelerated by an acceleration (**a**) given by the sum of these forces: driving force (Selfweight + Seismic forces) + lateral pressure + shear resistance

$$am = (W + Fv + Fx + Fy) + \left(\frac{\partial Px}{\partial x} \Delta x + \frac{\partial Py}{\partial y} \Delta y \right) + R \qquad (1)$$

Here, **R** includes the effects of forces of *N* and *U* in Fig. 1 and works in the upward direction of the maximum slope line before motion and in the opposite direction of landslide movement during motion.

The angle of slope is different in the position of column within landslide mass. All stresses and displacements are projected to the horizontal plane and calculated on the plane (Sassa 1988).

Figure 2 shows the projection of gravity (*g*) and vertical seismic acceleration (*gKv*), and horizontal seismic acceleration acting in *x* (*gKx*) and *y* directions (*gKy*). Here, *Kv*, *Kx*, *Ky* are seismic coefficients to the vertical, *x* and *y* directions, respectively.

Expressing Eq. 1 in *x* and *y* directions, Eqs. 2 and 3 are obtained. Assuming the total mass of landslide does not change during motion, (namely the sum of landslide mass flowing into a column (*M*, *N*) plus the increase of height of soil column is zero), Eq. 4 is obtained.

Equations 2, 3, and 4 are those obtained by Sassa 1988 plus the effects of triggering factors of earthquakes and pore water pressure.

$$\frac{\partial M}{\partial t} + \frac{\partial}{\partial x}(u_o M) + \frac{\partial}{\partial y}(v_o M) = gh \left\{ \frac{\tan \alpha}{q+1}(1 + Kv) + Kx \cos^2 \alpha \right\}$$
$$- (1 + Kv)kgh\frac{\partial h}{\partial x} - \frac{g}{(q+1)^{1/2}} \cdot \frac{u_o}{(u_o^2 + v_o^2 + w_o^2)^{1/2}} \{ h_c(q+1)$$
$$+ (1 - r_u)h \tan \phi_a \} \qquad (2)$$

$$\frac{\partial N}{\partial t} + \frac{\partial}{\partial x}(u_o N) + \frac{\partial}{\partial y}(v_o N) = gh \left\{ \frac{\tan \beta}{q+1}(1 + Kv) + Ky \cos^2 \beta \right\}$$
$$- (1 + Kv)kgh\frac{\partial h}{\partial y} - \frac{g}{(q+1)^{1/2}} \cdot \frac{v_o}{(u_o^2 + v_o^2 + w_o^2)^{1/2}} \{ h_c(q+1)$$
$$+ (1 - r_u)h \tan \phi_a \} \qquad (3)$$

$$\frac{\partial h}{\partial t} + \frac{\partial M}{\partial x} + \frac{\partial N}{\partial y} = 0 \qquad (4)$$

h	Height of soil column within a mesh
g	Gravity (acceleration)
α, β	Angles of the ground surface to *x–z* plain and *y–z* plain, respectively
u_o, v_o, w_o	Velocity of a soil column to *x*, *y*, *z* directions, respectively (velocity distribution in *z* direction is neglected, and regarded to be a constant)
M, *N*	Discharge of soil per unit width in *x*, *y* directions, respectively ($M = u_0 h, N = v_0 h$)
k	Lateral pressure ratio (ratio of lateral pressure and vertical pressure)
$\tan \phi_a$	Apparent friction coefficient mobilized at the sliding surface of landslide
hc	Cohesion *c* expressed in the unit of height ($c = \rho g$ hc, ρ: density of soil)

Fig. 1 Basic Principle of *LS-RAPID*. *Left*, a column element within a moving landslide mass. *Right*, balance of acting forces on a column
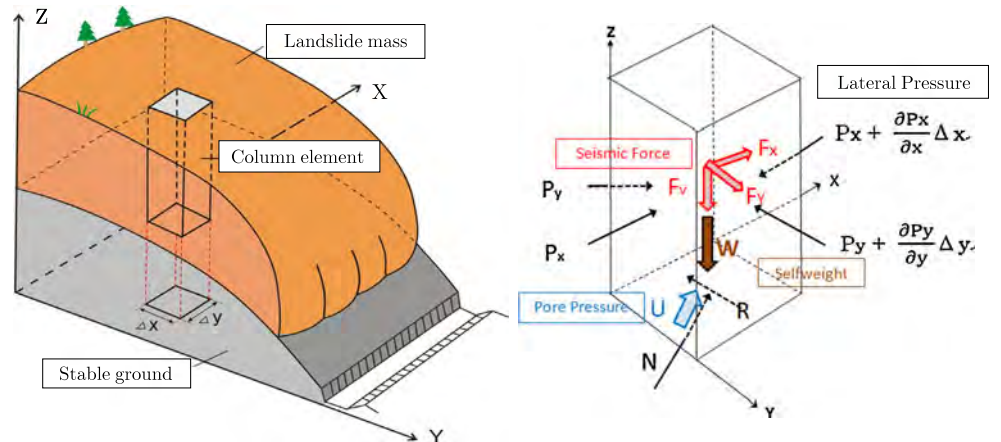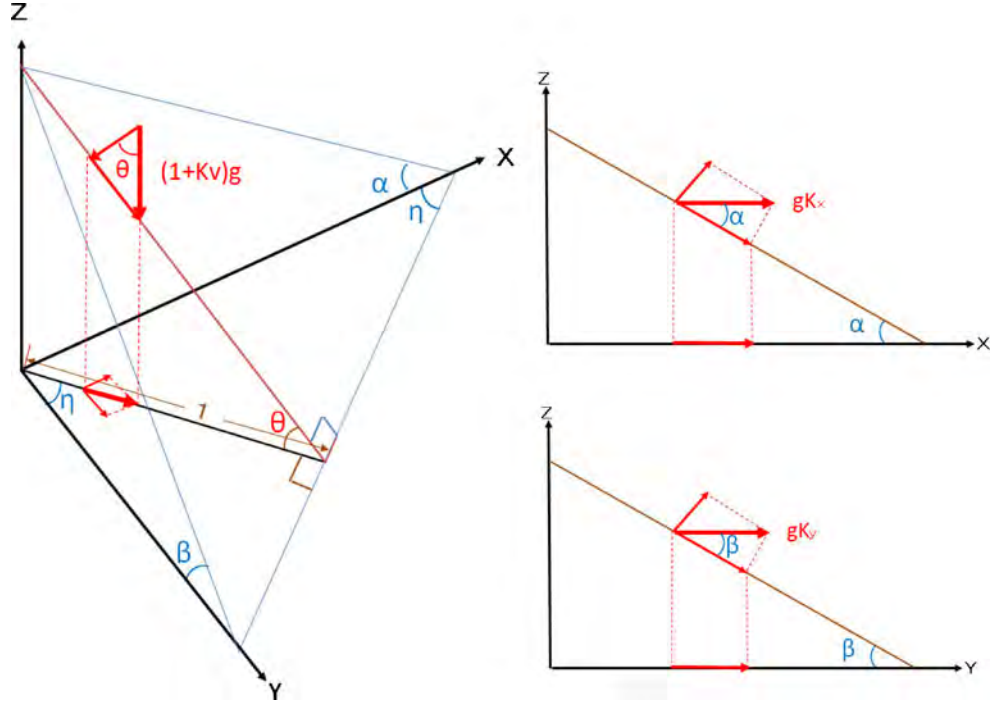
Fig. 2 Projection of seismic forces onto the horizontal plane. *Left,* gravity and vertical seismic force. *Right,* horizontal seismic forces (x and y directions)

$$q = \tan^2\alpha + \tan^2\beta$$

$$w_o = -(u_o \tan\alpha + v_o \tan\beta)$$

Kv, Kx, Ky Seismic coefficients to the vertical, x and y directions

r_u Pore pressure ratio (u/σ)

Explanation of k

The lateral pressure ratio (k) is the ratio between the horizontal stress (σ_h) and vertical stress (σ_v), namely $k = \sigma_h/\sigma_v$. k value in this model is expressed using the Jakey's equation (Sassa 1988).

$$k = 1 - \sin\phi_{ia} \qquad (5)$$

Here, $\tan\phi_{ia} = (c + (\sigma - u)\tan\phi_i)/\sigma$

$\tan\phi_{ia}$: Apparent friction coefficient within the landslide mass.

$\tan\phi_i$: Effective friction within the landslide mass (it is not always the same with the effective friction during motion on the sliding surface ϕ_m)

In the liquefied state, $\sigma = u, c = 0, then, \sin\phi_{ia} = 0, and\ k = 1.0$

In the rigid state, c is big enough, then $\sin\phi_{ia}$ is close to 1.0, then k is close to 0.

Explanation on ϕ_a, h_c, r_u

Equations 2, 3 and 4 can be established in both processes of initiation and the motion. The value of ϕ_a, h_c, r_u will vary in three states: (1) pre-failure state before the shear displacement at failure (start of strength reduction), (2) steady state after the end of strength reduction. (3) Transient state between the above both states. Those relations are examined later together with other factors and defined in Eqs. 10, 11, and 12.

Explanation of the seismic effects

Figure 2 illustrates the projection of vertical and horizontal seismic acceleration onto the horizontal plane.

The self-weight and vertical shaking work vertically on the column. The normal component of acceleration is cancelled out by the normal stress from the stable ground as the reaction. The component of acceleration parallel to the slope is remained and acts on the direction of the greatest slope inclination (θ). From the geometric relation, the horizontal component of gravity (1)+ seismic coefficient (Kv) to x and y directions are $g\frac{\tan\alpha}{q+1}(1 + Kv)$ and $g\frac{\tan\beta}{q+1}(1 + Kv)$, respectively.

x, y components of horizontal acceleration are $gKx \cos^2\alpha$, $gKy \cos^2\beta$, respectively.

The vertical shaking increases the vertical stress and the lateral pressure by (1+Kv). While the horizontal shaking does not increase the lateral pressure because the same force will act in the neighboring columns.

Apparent friction coefficient (tan ϕ_a)

The stresses acting on the sliding surface changes due to pore pressure rise during rainfalls or/and earthquakes. When the effective stress path moves from the initial point and reaches the failure line at peak (ϕ_p), the landslide movement will start. Pore pressure will be generated in progress with shear displacement in saturated soils when volume reduction will occur due to grain crushing/particle breakage. In this case the stress path

continues to go down along the failure line to a steady state along the failure line during motion (ϕ_m) below which any further grain crushing and pore pressure reduction will not occur. Only shear displacement will proceed under a constant shear resistance (steady-state shear resistance) as shown in Fig. 3.

The following relation is established in this state.

$$\tau_{ss} = \sigma_{ss} \tan \phi_m = \sigma_o \tan \phi_{a(ss)} \qquad (6)$$

τ_{ss}, σ_{ss} Shear stress and normal stress at the steady state.
$\tan \phi_{a(ss)}$ Apparent friction coefficient at the steady state

Therefore, the apparent friction coefficient at the steady state is expressed by the ratio of steady-state shear resistance (τ_{ss}) and the initial normal stress acting on the sliding surface (σ_o), which corresponds to the total normal stress (σ) due to soil weight at the site in the simulation

$$\tan \phi_{a(ss)} = \tau_{ss}/\sigma \qquad (7)$$

In a material and a state where pore pressure generation will not occur after failure, steady-state stress is not different from the stress at failure. The relation of Eq. 7 can stand in this case, too.

Effect of shear strength reduction from the prefailure state to the steady-state motion

The initiation process of this model consists of the following four sub-processes.

1. Initial state in which soil layer exists in a stable condition under the friction coefficient at peak (tan ϕ_p)
2. Failure (the instance of peak shear resistance) will occur due to the rise of ground water level during rains, seismic loading during earthquakes, or the combination of ground water rise and seismic loading

3. Transient state from peak to steady state in which pore pressure generation and resulting shear strength reduction will proceed in progress with shear displacement
4. Steady state in which the landslide mass moves with no further strength reduction.

Figure 4 presents examples of test results of silica sands in use of the undrained ring shear apparatus (Igwe et al. Igwe et al. 2007). Shear resistance reaches its peak value within 1–2 mm shear displacement, and both cases reaches a steady state between 10–5,000 mm shear displacement. Strength reduction after 1,000 mm is very small, so it will be regarded to reach steady state between 10–1,000 mm.

In references to these experimental results, the shear behavior from the pre-failure state to a steady state of motion through the transient state was approximated in the way shown in Fig. 5. Namely the friction angle at peak (ϕ_p) is kept in the pre-failure state until the shear displacement DL (Point of failure, Start of strength reduction). In the real slopes shear stress does not start from zero. It is relatively close to the peak though the level is unknown. Shear strength will reduce from DL to DU (End of strength reduction) in the shear displacement along a line in the logarithmic axis. A steady-state landslide motion will start under the apparent friction coefficient at steady state (tan $\phi_{a(ss)}$) after DU in the shear displacement. Expressing the shear displacement as D, the friction coefficient has three stages below.

1. Initial deformation stage before failure (D<DL): $\tan \phi_a = \tan \phi_p$
2. Stage of steady-state motion (D>DU): $\tan \phi_a = \tan \phi_{a(ss)}$
3. Stage of transient state (DL<D<DU): $\tan\phi_a = \tan\phi_p - \frac{\log D - \log DL}{\log DU - \log DL}\left(\tan\phi_p - \tan\phi_{a(ss)}\right)$

Effect of soil depth on the apparent friction coefficient

The normal stress at the steady state (σ_{ss}) is independent of the level of loaded normal stress. Figure 6 is an example of weathered granitic soils taken from Osaka formation in which the Nikawa landslide killing 34 persons in Nishinomiya city, Hyogo Prefec-

Fig. 3 Apparent friction coefficient (tan ϕ_a), steady-state shear resistance (τ_{ss}) and the friction coefficient during motion (tan ϕ_m)
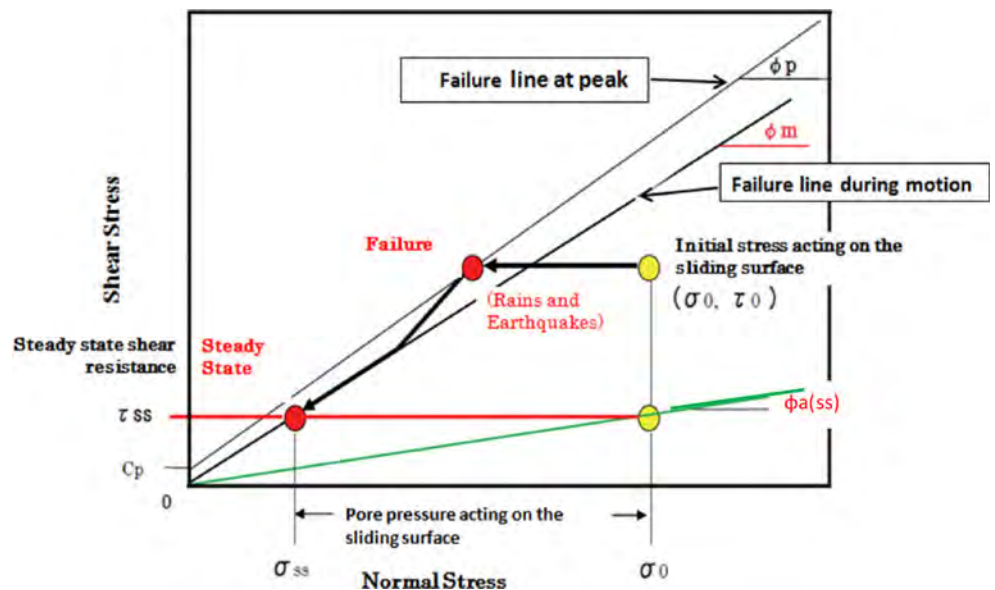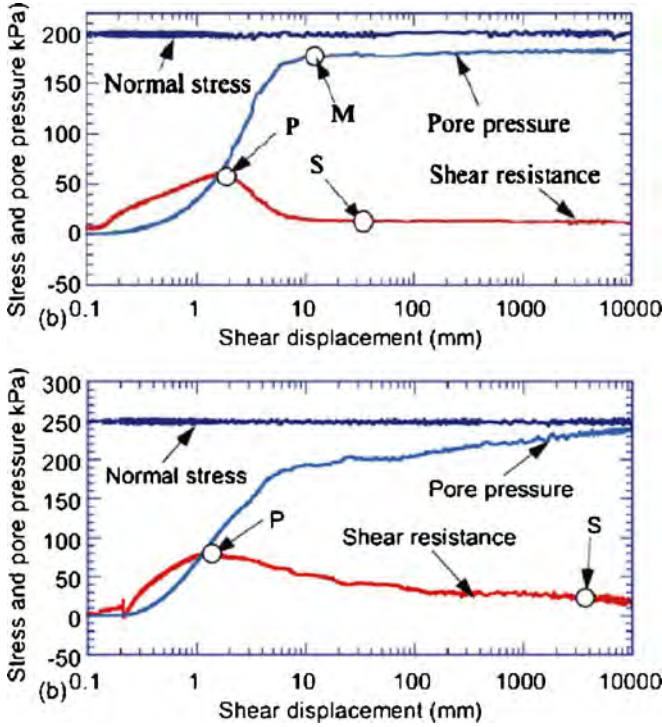
Fig. 4 Relationship between shear resistance shear displacement of silica sands (Igwe et al. 2007)

ture, Japan occurred. All soils with different normal stress reached the same steady-state shear resistance in the undrained ring shear test. No further grain crushing and volume reduction will not occur under this critical normal stress. Using this relation, the apparent friction coefficient will be decided in the way illustrated in Fig. 7 when the soil depth will change. In the state of greater depth of landslide mass, the mobilized apparent friction coefficient (τ_{ss}/σ_A) is smaller as shown in the point A. However, as the depth of landslide mass becomes smaller, the mobilized friction coefficient becomes greater as shown in the point B. In the lower normal stress than the normal stress at steady state (σ_{ss}), the apparent friction coefficient is same with the friction coefficient during motion (tan ϕ_m) as shown in the point C. When the motion of landslide mass is accelerated and moves fast, the landslide depth will decrease, in this case the apparent friction coefficient will increase.
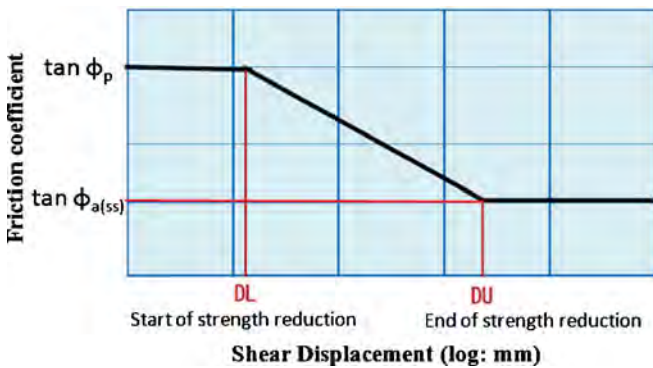

Fig. 5 Model of shear strength reduction in progress of shear displacement

Effect of saturation on the apparent friction coefficien

Pore water pressure generation is affected by the degree of saturation. In the triaxial test, the relationship between pore water pressure parameter $B = \Delta u/\Delta\sigma_3$ and the degree of saturation (Sr) is approximately expressed in the small increment of confining pressure by Eq. 8 (Sassa 1988). Figure 8 is the relationship between the B-value and the degree of saturation which was obtained by the isotropic triaxial compression tests on the torrent deposits in the 1984 Ontake debris avalanche in different degree of saturation. The correlation between the B value and the degree of saturation, i.e., the solid line shown in Fig. 8 can be expressed in the form of Eq. 8, which is almost same with the experimental plots.

$$B = \frac{1}{1 + \frac{n}{Cc_3}\left\{\frac{Sr}{100}Cw + \frac{100-Sr(1+\alpha B\Delta\sigma_3)}{100} \cdot \frac{1}{u_o+B\Delta\sigma_3}\right\}} \qquad (8)$$

Here, Sr, degree of saturation; n, porosity; Cc3, three dimensional compressibility of soils

Cw, Compressibility of water; α, Constant for absorption of air into water (Henry's law)

u_o, Initial pore pressure including atmospheric pressure; $\Delta\sigma_3$, increment of confining pressure

The apparent friction coefficient is affected by the degree of saturation of soils. We will use a parameter of pore pressure generation rate B_{ss} which is very similar to pore pressure parameter B, though B is defined in the undrained isotropic compression triaxial test while B_{ss} is defined in the undrained ring shear test.

In Fig. 9, we will denote the steady-state shear resistance at full saturation as τ_{ss} (B_{ss}=1.0) and the steady state at dry state as τ_{ss} (B_{ss}= 0.0). If the percentage of pore pressure generation is 60% of the full saturation, the steady state is denoted as τ_{ss} (B_{ss}=0.6). As found in Fig. 9, the apparent friction angle ϕ_a (dr)=ϕ_m in the dry state. ϕ_a(fs) at full saturation is the lowest, ϕ_a(ps) at partial saturation is in between.

### Landslide triggering in the source area

Calculation of shear displacement and time step

During rains and earthquakes, seismic stresses will act on the potential landslide body and pore pressure will act on the potential sliding surface, then, trigger a landslide. We focus on the seismic force and pore pressure in the source area. We will designate the source area within the whole simulation area in advance. Seismic force and pore pressure rise are given only in the soil mass in the source area. The detailed pore pressure distribution is not known, then pore pressure ratio (r_u) is increased gradually. When those triggering factors will be loaded, no or a certain shear displacement will occur in each mesh. Shear displacement (D) at each mesh is calculated from the sum of (velocity of each step) x (time step of each step) in x direction and the sum in y direction for a specific mesh in the following equation.

$$D = \left\{\left(\sum_{i=1}^{i} U(i) \cdot \Delta t(i)\right)^2 + \left(\sum_{i=1}^{i} V(i) \cdot \Delta t(i)\right)^2\right\}^{1/2} \qquad (9)$$

Here, U, V are velocity in the x and y directions at a specific mesh and a specific time step

Fig. 6 Undrained ring shear tests on the Osaka Formation in which Nikawa landslide disaster occurred at the 1995 Hyogoken Nambu Earthquake (Okada et al. 2000)
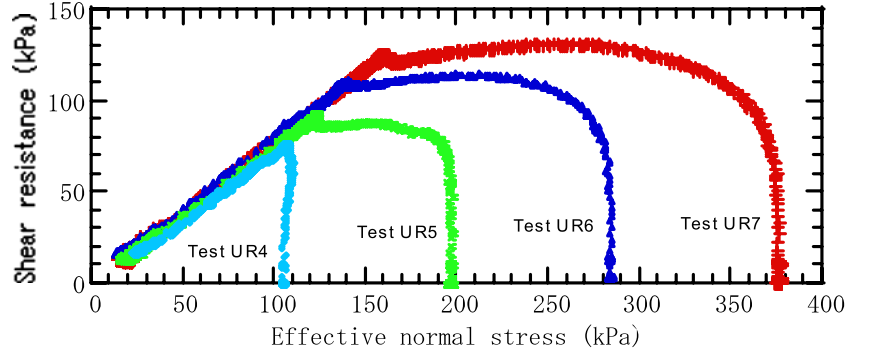
Time step in *LS-RAPID* is not a constant. It is decided to obtain a precise necessary calculation either in the initiation process before the steady state and also in the steady-state motion.

$$\Delta t = DU/M/(Umax^2 + Vmax^2)^{1/2} \text{ in the initiation process.}$$

DU, shear displacement at the end of strength reduction; *M*, necessary number of calculation steps (10 was given for an imaginary simple slope and 20 given for the Leyte landslide in the calculation of this paper); Umax, Vmax, maximum velocity at each step.

But the initial time step must be given because velocity is not yet calculated. 0.005 s was given in this calculation.

The time step in the steady state is decided by the size of mesh and how many times calculation is necessary to obtain precise value. It depends on the velocity and the size of mesh.

$\Delta t = dx/N/V$ in the steady-state motion

dx, size of mesh. *N*, necessary number of calculation steps (10 was given for an imaginary simple slope and 20 given for the Leyte landslide); *V*, the greater maximum velocity within Umax and Vmax calculated at the latest step.

Effect of pore pressure ratio to shear resistance in the initiation process
Effect of excess pore pressure generated during shear is included in the value of the apparent friction coefficient tan $\phi_{a\,(ss)}$ in the steady state ($D>DU$). However, effect of pore pressure due to

ground water rise due to rains is not considered in the apparent friction coefficient in the range of $D<DL$. The transient phase in $DL<D<DU$ are both partly working. The effects of pore pressure ratio (r_u) together with the apparent friction coefficient (tan ϕ_a) in three stages are written as below,

1. $D < DL$: $\tan\phi_a = \tan\phi_p$, $c = c_p$, $r_u = r_u$ (10)

2. $D > DU$: $\tan\phi_a = \tan\phi_{a(ss)}$, $c = 0$, $r_u = 0$ (11)

3. $DL \le D \le DU$: $\tan\phi_a = \tan\phi_p - \dfrac{\log D - \log DL}{\log DU - \log DL}(\tan\phi_p - \tan\phi_{a(ss)})$,

$$c = c_p\left(1 - \frac{\log D - \log DL}{\log DU - \log DL}\right), \quad r_u = r_u \cdot \frac{\log DU - \log D}{\log DU - \log DL}$$ (12)

When and where shear displacement calculated by Eq. 9 reaches *DL*, shear strength reduction will start. When and where shear displacement reaches *DU*, the steady-state movement will start. The movement area will progressively enlarge because of shear strength reduction.
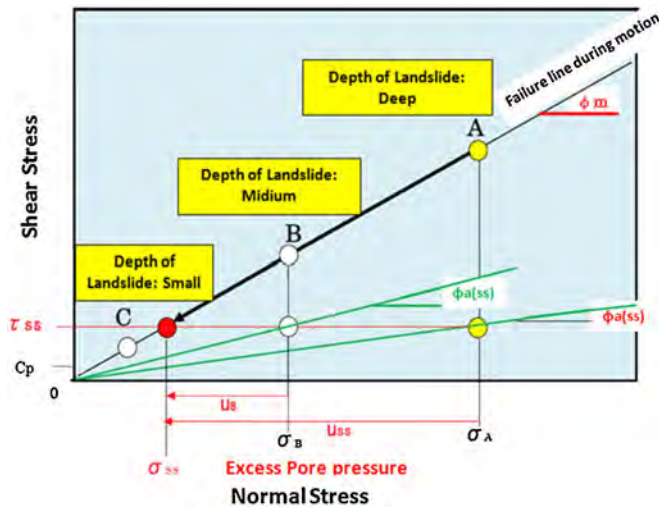

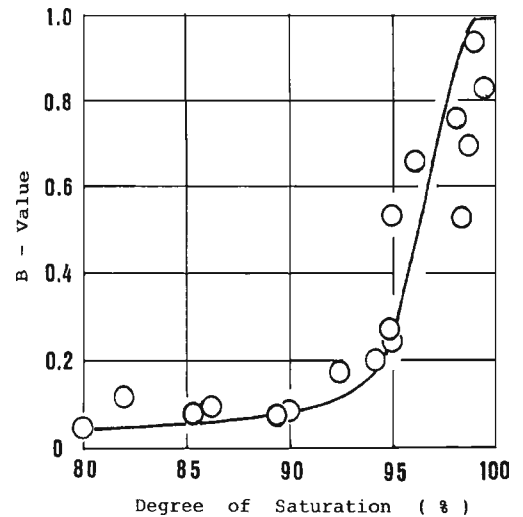**Fig. 7** Effect of soil depth to the apparent friction angle

Fig. 8 Correlation between the B-value and the degree of saturation on the torrent deposits in the 1984 Ontake debris avalanche (Sassa 1988)
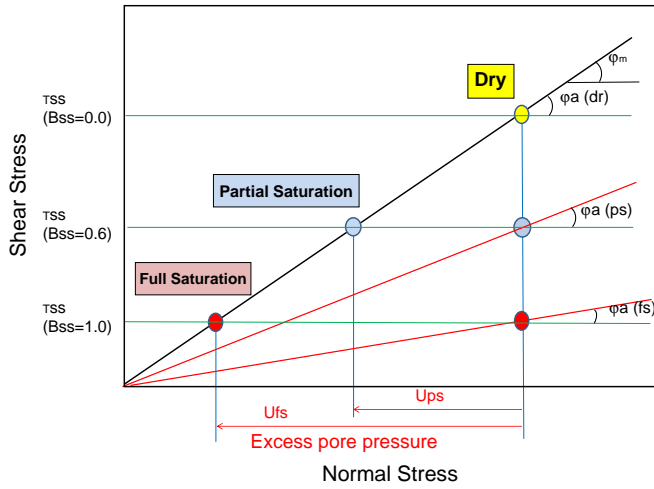
Fig. 9 Relationship between the pore pressure generation rate (B_{ss}) and the apparent friction coefficient

Landslide enlargement in the entrainment area

The landslide volume often increases during motion by entraining unstable deposits located in the travel course. This phenomena will be observed in such cases, (1) a small landslide occurs in the upper slope and it is gradually enlarged during the down slope movement by scraping weathered soils or pumice and other unstable deposits, or a landslide mass enters into a torrent, and entraining torrent deposits by undrained loading, (2) a large scale landslide mass which occurred in a steep slope goes on to the alluvial deposit in which a saturated layer often exist under the ground. The alluvial deposit is sheared within the saturated layer, and entrained into the moving landslide mass.

We have assumed the following in this volume enlargement model. When a landslide mass greater than a certain height of thickness rides on an unstable soil layer, the friction coefficient within the unstable deposit will change from the friction coefficient at peak (tan ϕ_p) and cohesion at peak (c_p) to the apparent friction coefficient (tan $\phi_{a(ss)}$) with no cohesion due to undrained loading and undrained shear resulted from the impact by the rapid moving landslide mass. The effect of impact is not easy to estimate. The same procedure to include shear resistance reduction with progress of shear displacement with the initiation model of landslides makes this simulation too complicate. So we made a volume enlargement model by simplifying this process as follows: the sudden reduction of shear strength from the peak friction to the apparent friction at the steady state will occur when a landslide mass greater that a certain threshold height of soil thickness (Δh_{cr}) reaches a mesh containing unstable deposits. In Fig. 10, when a landslide mass comes, the height of soil column in this entrainment area increases from h_d to ($h_d + h_m$). If the height of landslide mass $h_m > \Delta h_{cr}$, the friction at the base of this column becomes that at the steady state. The basic Eqs. 2, 3, and 4 are effective for each mesh in the entrainment area. Only difference is the height of soil column is the total of landslide mass and the unstable deposit. How much deposit is entrained or how much landslide mass deposits on the entrainment area will appear as the result of this calculation by Eqs. 2, 3, and 4.

Figure 11 (top) illustrates the undrained loading by a falling landslide mass from the slope onto the torrent deposit. Figure 11
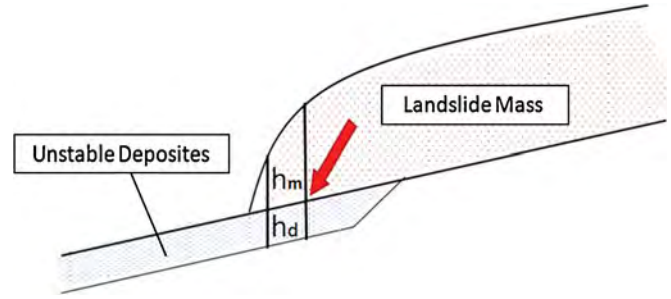

Fig. 10 Undrained loading onto deposits by the moving landslide mass in its traveling course

(bottom) is the test result to reproduce this process by undrained dynamic loading ring shear apparatus (Sassa et al. 2004a). The impact stress was given for 5 s during which the shear stress and normal stress were rapidly increased. Thereafter, normal stress was kept constant due to the increase of self-weight (corresponding to $\alpha = 0$ in the top figure), while shear stress was reduced from the impact stress until the component of increased self-weight (the landslide mass + torrent deposit). The monitored pore water pressure and mobilized shear resistance and the resulting accelerated shear displacement were shown in the graph (b). It presented the unstable mass started to move by this undrained impact loading and the torrent deposit was entrained and the volume of landslide enlarged.

Resistance due to non-frictional energy consumption

The basic equation of 1 is based on the assumption in which all potential energy is consumed as the frictional energy at the sliding surface during motion. However, the landslide mass may lose kinetic energy during collision of sub-masses within a landslide mass, momentum transfer to engulfed materials and the movement passing over vertical gaps/falls, horizontal bent or other not-smooth ground surface. In these instances and locations, the assumption of all energy is consumed as friction cannot stand. In this case, an extraordinary velocity or an extraordinary thickness of soils will appear as the result of calculation of Eqs. 2, 3, and 4. It misleads a wrong simulation result. To avoid this case automatically, energy loss function is incorporated for a specific mesh and a specific time step by the threshold values of extraordinary velocity or/and thickness. The major part of non-frictional energy consumption will be the loss of kinetic energy. The most common idea is to use the energy loss term proportional to the kinetic energy of the soil mass at a mesh ($\frac{1}{2}mv^2$)

Namely, the non-frictional energy consumption in a column

$$= \alpha \left(\frac{1}{2} mv^2 \right) \tag{13}$$

m, soil mass within a column at the mesh; v, velocity at the mesh; α, Coefficient for non-frictional energy consumption (constant with dimension of reciprocal of length)

$$am = (W + Fv + Fx + Fy) + \left(\frac{\partial Px}{\partial x}\Delta x + \frac{\partial Py}{\partial v}\Delta y \right) + R + \alpha \left(\frac{1}{2}mv^2 \right) \tag{14}$$
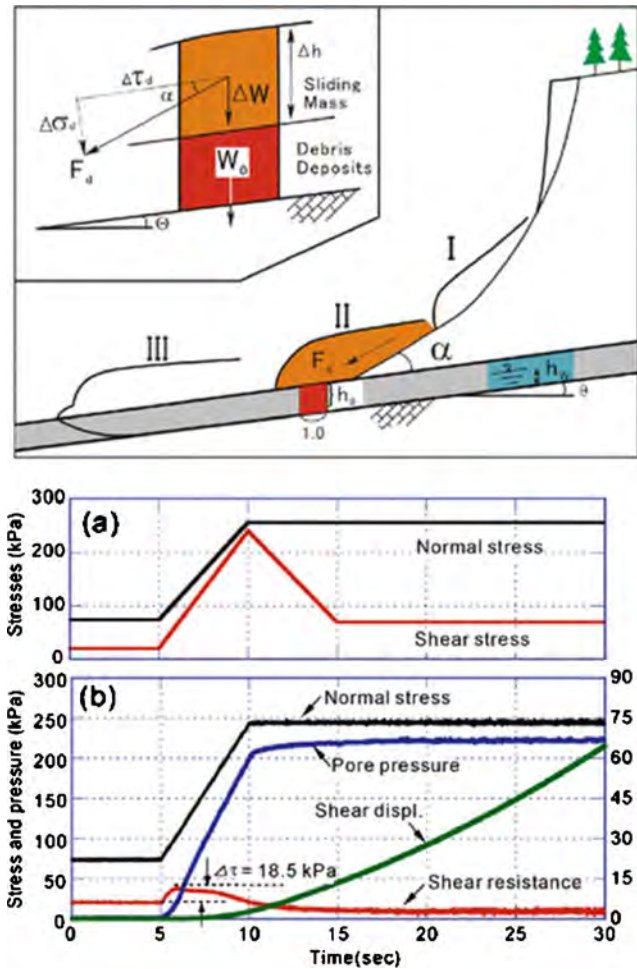
Fig. 11 Illustration of the impact loaded by the falling landslide mass onto the deposits (*top*) and the result of undrained ring shear test simulating this process (*bottom*) (Sassa et al. 2004a)

The last term functions only at a mesh and at an instance when an extraordinary velocity or/and soil height will appear. The soil height and velocity will be recovered to the range below the extraordinary values, the function will stop. If a single step of calculation at a mesh will lead a negative soil height, it is regarded to be zero. In the trial test, in simple slopes, this function was not triggered. The landslide distribution and the time of movement was the same with this function and without this function. In the case of the complicate large scale landslide in the Leyte landslide, α=0.2, 1.0, 2.0, 5.0, 10.0 gave almost same simulation result. But in the case of α=0, at a specific mesh and a specific time, velocity exceeded hundreds m/sec and the simulation result was different from the natural phenomena and others (α=0.2, 1.0, 2.0, 5.0, 10.0). Then, α=1.0 was used in the simulation of the Leyte landslide.

Voellmy (Körner 1980 or others) proposed the shear resistance R will be the sum of the resistance by Solid (R_{solid}) due to friction and the resistance by Fluid (R_{fluid}) in proportion to square of velocity. A coefficient (ξ) "Turbulent coefficient" was used to express the shear resistance due to Fluid. This concept is currently used for the simulation of landslides. In the 2007 benchmarking exercise, most groups (eight out of 13) included the Voellmy's model (the resistance due to the square of velocity plus the resistance due to friction)

through the simulation. In the computer simulation *LS-RAPID*, the apparent friction will increase in smaller depth of landslide mass at a greater velocity movement automatically. It works similarly to increase resistance during a high speed motion. The authors think the velocity dependent energy loss is not necessary through the whole process of simulation in the model of *LS-RAPID*. The loss of non-frictional kinetic energy due to collision or so needs to be incorporated for a specific site (mesh) at specific time. Soil height and velocity at each step and each mesh are used as Index informing this situation.

Examination of the performance of each process
The performance of each process of *LS-RAPID* is examined by applying it to a simple imaginary slope. The imaginary slope which is composed of three parts of slope; a flat ground in the top, a steep slope in the middle and a gentle slope in the bottom. The area of simulation is 350 m wide and 440 m long, the size of mesh is 10 m, the maximum vertical depth of landslide is 40.53 m, the total landslide volume is 231,300 m³. The landslide body was created in a form of ellipsoid which is explained in the application to the Leyte landslide using Fig. 20.

Initiation process
The initiation process by pore pressure increase on the initiation of rapid landslides was firstly examined.

The characteristic of *LS-RAPID* is the expression of strength reduction during deformation and the progressive failure. A relatively strong slope was considered which may be failed by a high pore pressure ratio supplied from the bed rock (Figs. 12 and 13) or a combined effect of seismic loading in addition to moderate pore pressure ratio (Fig. 14).

The values of tan ϕ_p=0.8, c_p=50 kPa, τ_{ss}=50 kPa, k=0.5, B_{ss}=0.99, tan ϕ_m=0.60 were given to all simulation area. As the parameters of the shear resistance reduction, the shear displacement at the start of reduction DL=10 mm, the shear displacement reaching to the steady-state shear resistance DU=1,000 mm were given in the reference of the result of undrained ring shear test (Fig. 4) for a probable case. A local failure and shear strength reduction may start at a mesh (site) in which the shear displacement firstly reaches DL=10 mm, then it may develop to a progressive failure.

In order to compare this simulation result to the limit equilibrium slope stability analysis such as Fellenius, Bishop, Janbu, Spenser, Morgenstern–Price, enough large shear displacement for DL and DU was given to be 2 and 5 m, respectively. The limit equilibrium slope stability analysis does not consider the progressive failure, but fails at once. The large shear displacement DL is effective to restrain the effect of shear resistance reduction and the progressive failure in the initiation process. The simulation results are shown in form of 3D view in Fig. 12. The contour line is 2.0 m pitch. The red color line shows the area of moving landslide mass. The red color will appear when/where the velocity at a mesh will exceed 0.5 m/s.

DL=10 mm, DL=1000 mm
In the case of r_u=0.4 (Fig. 12a), only two small areas on the top of slope showed a slight movement and two red colored circles were observed, but no further progressive failure appeared.

For r_u=0.5 and 0.6 rapid landslide motion appeared as shown in Fig. 12c, e.

$DL=2{,}000$ mm, $DU=5{,}000$ mm
No motion appeared for $r_u=0.4$, a limited deformation appeared for an instant in the case of $r_u=0.5$ as shown Fig. 12b, d. A rapid landslide occurred for $r_u=0.6$ (Fig. 12f). The border of landslide initiation is between $r_u=0.4$ and 0.5 for smaller DL–DU, and it is between 0.5 and 0.6 for greater DL–DU.

Time

Simulation will stop when the zero velocity for all meshes appeared. Time in the figure shows the time from the start to the end of motion. Ten seconds for A, B, D is the pre-decided minimum calculation time, because the initial velocity is zero, and a certain time of calculation is necessary to know movement will start or not.

For the central section of this landslide mass, two dimensional slope stability analyses were implemented using the stability analysis software "Slide version 5" by Rocscience. The same shear strength parameters at the peak and also the same pore pressure ratio (tan $\phi_p=0.8$, $c_p=50$ kPa, $r_u=0.4$, 0.5, 0.6) were given for all stability analysis methods. The calculated safety factors for 1: Fellenius, 2: Bishop simplified, 3:Janbu simplified, 4: Spenser, 5: Morgenstern–Price were shown in the right column of Fig. 12. The onset of landslide motion, namely the unit safety factor (FS=1.0) appears when the value of r_u is between 0.5 and 0.6 for four models. For the Fellenius method, the factor of safety becomes unity when the value of r_u is between 0.6 and 0.7. Therefore, the border of stability (FS=1.0) is same with the border by *LS-RAPID* in the case of long shear displacement (2 m) until the start of shear strength

reduction except the Fellenius method. The difference between *LS-RAPID* and the Limit Equilibrium Slope stability Analysis comes mainly from the consideration of local shear and progressive failure or the overall shear for the whole landslide body at once. The difference between three dimensional analysis (LS-RAPID) and two dimensional analysis is not possible to be discussed in this examination.

Moving process

Two key parameters for this simulation are *steady-state shear resistance* (τ_{ss}) and *lateral pressure ratio* (k). τ_{ss} controls how far a landslide mass moves. The lateral pressure presents the softness of soil mass. A–D of Fig. 13 visualized the results of motion for two different steady state ($\tau_{ss}=40$ kPa, 60 kPa) and two different lateral pressure ratio ($k=0.3$ and 0.8). Two cases (B and D) of smaller steady state ($\tau_{ss}=40$ kPa,) traveled longer than two cases (A and C) of greater steady state ($\tau_{ss}=60$ kPa). While two cases (C and D) of greater lateral pressure ratio ($k=0.8$) presented wider lateral movement than two cases (A and B) of smaller lateral pressure ratio ($k=0.3$). The deposit shape was more flat and smooth in cases with greater lateral pressure ratio.

When a landslide mass travels on unstable deposits in the traveling course, sometimes those deposits are entrained by shearing illustrated in Figs. 10 and 11.The effect was investigated by adding unstable deposits on the flat area in the case of Fig. 13e; 5 m deposits were located on the flat area (usually alluvial deposits). The results of movement and the longitudinal section and the cross section were also presented. Comparing to Case A (same steady-state shear resistance and lateral pressure ratio), the volume was increased and
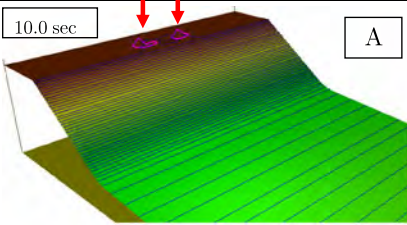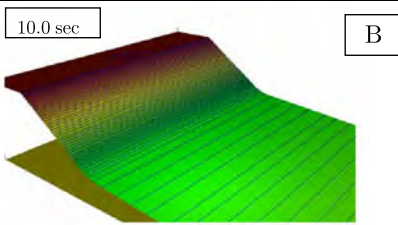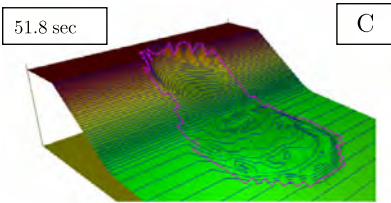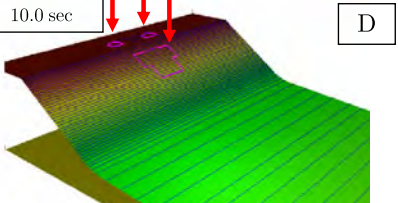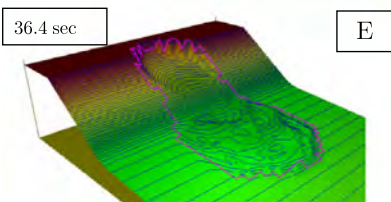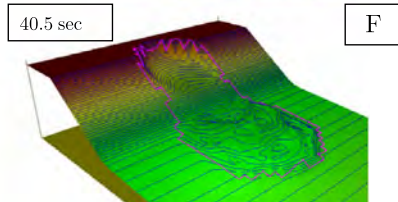
PP ratio r_u	Landslide simulation RAPID		Slope stability analysis				
	DL=10mm, DU=1000mm	DL=2000mm, DU=5000mm	Fel. (*1)	Bisp (*2)	Jan (*3)	Spn (*4)	M&P (*5)
0.4	10.0 sec A	10.0 sec B	1.545	1.443	1.381	1.433	1.431
0.5	51.8 sec C	10.0 sec D	1.351	1.207	1.151	1.200	1.199
0.6	36.4 sec E	40.5 sec F	1.155	0.973	0.923	0.970	0.970

Fig. 12 Landslide initiation in *LS-RAPID* and Slope Stability Analysis. tan $\phi_p=0.8$, $c_p=50$ kPa, $\tau_{ss}=50$ kPa, $k=0.5$, $B_{ss}=0.99$, tan $\phi_m=0.60$, $\alpha=0$, mesh, 10 m; area, 350×440 m; contour line, 2 m. *1 Fellenius, *2 Bishop simplified, *3 Janbu simplified, *4 Spenser, *5 Morgenstern–Price
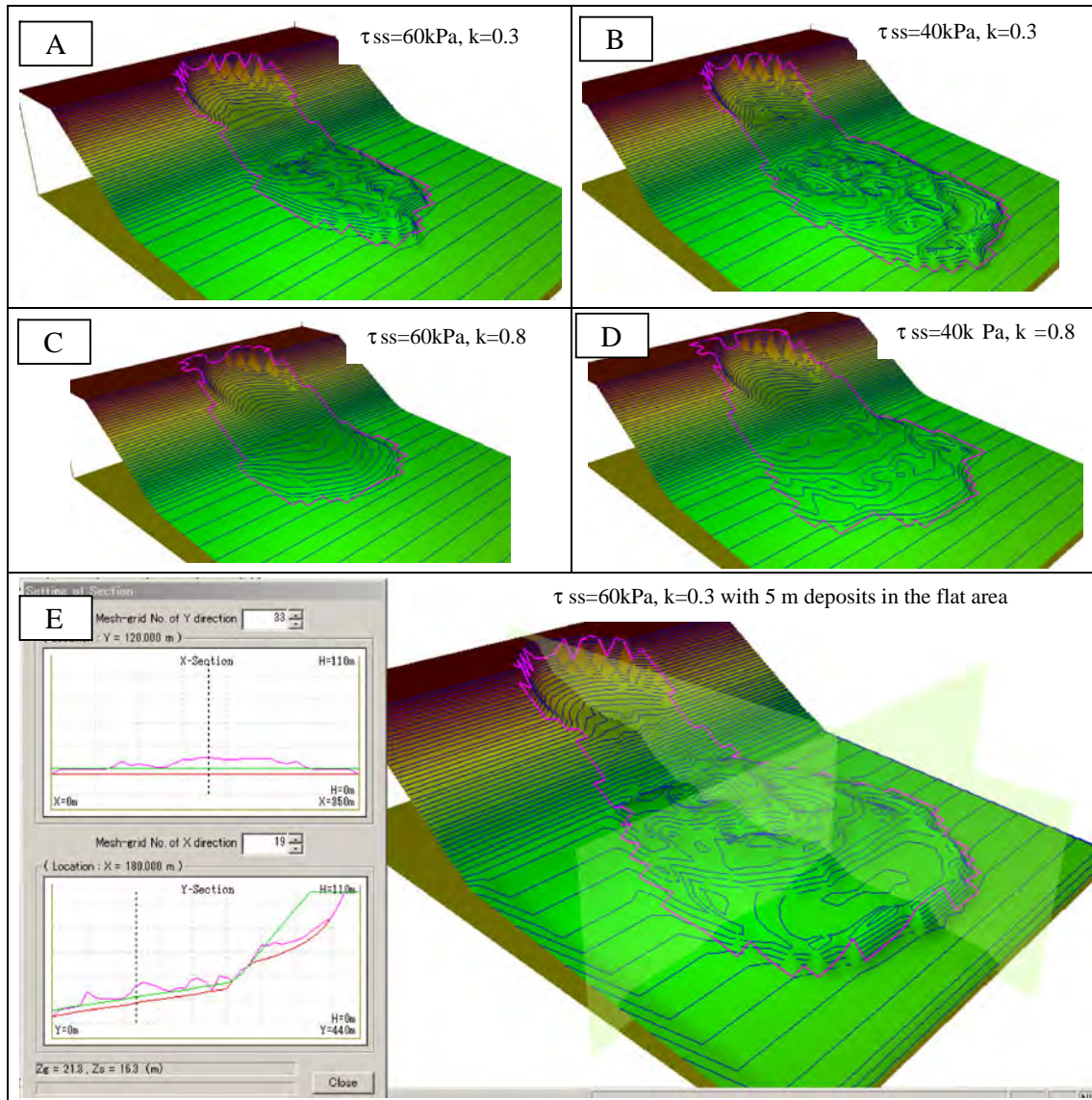
Fig. 13 Effects of steady-state, lateral pressure ratio, and unstable deposits in the traveling ground. tan ϕ_p=0.8; c_p=50 kPa; τ_{ss}=40 kPa and 60 kPa; k=0.3 and 0.8; r_u=0.5; B_{ss}=0.99; tan ϕ_m=0.60; α=0; DL=10 mm; DU=1,000 mm; mesh, 10 m; area, 350×440 m)

the movement area was increased. The transparent plates presented the location of longitudinal and crossing sections which are shown in the right side of Fig. 13e. The green color is the original ground surface. The difference of colors are not clear in this small figure. The dense red color presents the bottom of unstable mass (alluvial deposit) on the flat area and the landslide mass in the source area. The pink color presents the surface of landslide mass after motion.

Combined effects of earthquake and pore pressure ratio

Landslides may be triggered by earthquakes and both effects of earthquakes and pore water pressure. The border between rapid landslide and no movement was examined by earthquake loading in addition to pore pressure ratio. The preliminary test proved that the pore pressure ratio r_u=0.4 does not cause landslide without earthquake loading though r_u=0.5 will cause a rapid landslide.

Then, to examine the combined effects of earthquake and pore pressure ratio, both triggering factors (as shown in Fig. 14) were

loaded in the same imaginary slope with Figs. 12 and 13. Firstly, the pore pressure ratio is increased from 0 to 0.4 during T=0–5 s. Then, cyclic loading was loaded from T=10–25 s with 1 Hz. The magnitude reaches the pre-decided value for three cycles and keeps the same magnitude for nine cycles and decreases to zero for three cycles. The same magnitude of horizontal shaking (Ky-landslide direction) and vertical shaking (Kv) were loaded while horizontal shaking in x direction (crossing direction to the landslide) was kept zero. Four test results are presented in Fig. 15 for two seismic coefficients and two sets of DL and DU just above/below the occurrence of rapid landslides. Fig. 15a, c presents the cases which local deformation are observed, but those stopped without further progressive failure. Fig. 15b, d presented the motion of rapid landslides. In the case of DL=10 mm, DU=1,000 mm, the critical seismic shaking was between Ky=Kv=0.08 and 0.09. In the case of DL=2,000 mm and DU=5,000 mm, the critical seismic shaking was between Ky=Kv=0.6 and 0.7. Therefore,
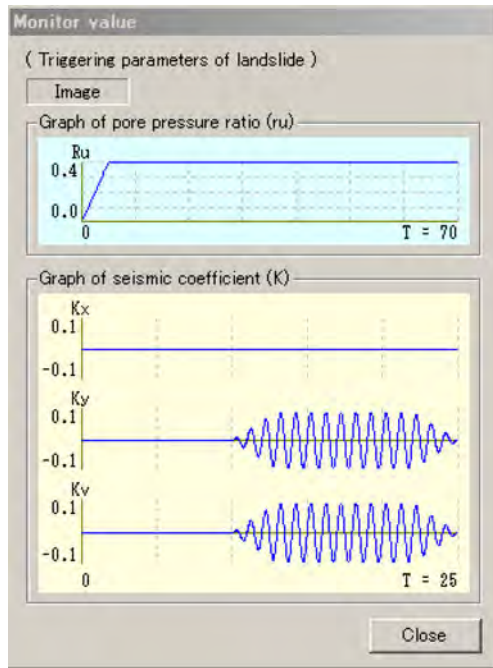
Fig. 14 Triggering factors (pore pressure ratio: r_u=0.4, cyclic loading: 1 Hz, total of 15 cycles for 10–25 s, Same seismic coefficient in horizontal shaking in y (landslide) direction (Ky) and vertical direction (Kv)

landslide risk during earthquakes are much affected by the threshold value of shear displacement to start the shear strength reduction as well as the magnitude of seismic shaking (seismic coefficient).

Application to the 2006 Leyte landslide

A rapid and long-traveling landslide occurred on 17 February 2006 in the southern part of Leyte Island, Philippines. The landslide caused 154 confirmed fatalities and 990 people missing in the debris. The International Consortium on Landslides (ICL) and the Philippine Institute of Volcanology and Seismology (PHIVOLCS) organized a joint Japanese and Philippine team of 22 scientists and engineers. The team investigated the landslide from the ground and from a chartered helicopter. The investigation was reported at the International Conference-Workshop "Guinsaugon 2008—Living with landslides" (Sassa, Fukuoka, Solidum et al. 2008). The results were presented as a part of paper on the combined effect of earthquake and rainfalls (Sassa, Fukuoka, et al. 2007). The landslide volume was 20 million m³ (Catane et al. 2007) and 16–30 million m³ (Araiba et al. 2008).

Figure 16 is a frontal view of the landslide taken from a helicopter. A planer hard rock is seen at the left side of the headscarp. Other parts of the slope seem to be weathered volcanoclastic rocks or debris. The landslide mass moved from the slope and deposited on the flat area. Many flow-mounds or hummocky structure were found. The features of this landslide were reported by Catane et al. 2007.

The section of the central line of the landslide was surveyed by a non-mirror total station and a ground-based laser scanner in the field and compared with a SRTM (Shuttle Radar Topography Mission) map before the landslide which was implemented by H. Fukuoka, a member of the team and colleagues from Philippines. The red-color part shows the initial landslide mass while the blue-color part presents the displaced landslide debris after deposition. The length of landslide from the head scar to the toe of the deposition is around 4 km. The inclination connecting the top of
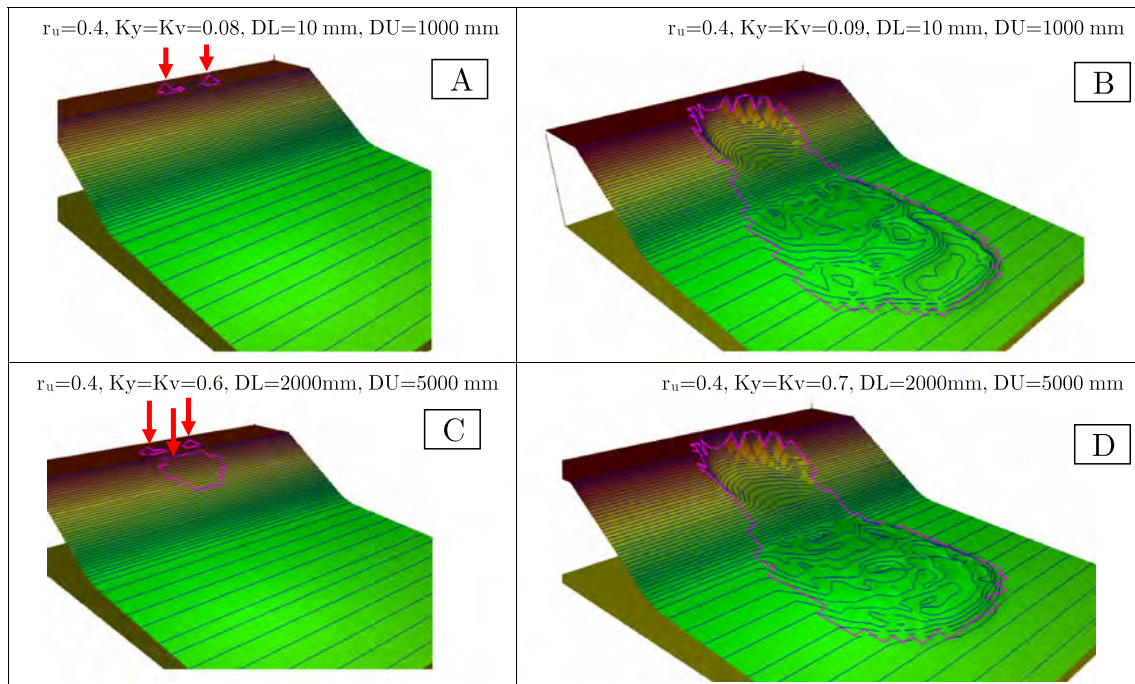

Fig. 15 Combined effects of seismic loading and pore pressure for different DU and DL and different seismic coefficients. (tan ϕ_p=0.8, c_p=50 kPa, τ_{ss}=50 kPa, k=0.5, B_{ss}=0.99, tan ϕ_m=0.60)

the initial landslide and the toe of the displaced landslide deposit is approximately 10°, which indicates the average apparent friction angle mobilized during the whole travel distance. The value is much smaller than the usual friction angle of debris (sandy gravel) of 30–40°. Therefore, it suggests that high excess pore-water pressure was generated during motion. Figure 17b shows a flow mound that traveled from the initial slope to this flat area without much disturbance. Movement without much disturbance is possible when the shear resistance on the sliding surface became very low; thus, movement of the material is like that of a sled.

The material of the flow mound is volcanoclastic debris, including sand and gravel. We observed the material in the source area by eye observation from the surface and by hand scoop excavation in the valley-side slope after the landslide. It consisted of volcanoclastic debris or strongly weathered volcanoclastic rocks. It is regarded to be the same material (either disturbed or intact) observed in the flow mound shown in Fig. 17. Therefore, we took a sample of about 100 kg from the base of the flow mound shown in the point "S" in the section of Fig. 17a) and the photo of Fig. 17b. The

location is in the center of travel course and just below the source area. Then, we transported the material to Japan and subjected it to the undrained dynamic-loading ring-shear test.

Testing apparatus

The undrained dynamic-loading ring-shear apparatus (DPRI-3) was developed from 1992 to 2004 (DPRI-7). The basic concept of this apparatus is to reproduce the formation of sliding surface and its post-failure motion by reproducing the stress acting on the sliding zone and to observe the generated pore water pressure, mobilized shear resistance and post-failure rapid motion. It can provide seismic stress in addition to gravity and pore-water pressure as triggering factors. The leakage of pore water from the edge of rotating half and stable half is prevented by a rubber edge which is pressed at a contact pressure greater than the pore water pressure inside the shear box by servo-control system. The apparatus used for this test is DPRI-6, which is capable to do tests under dynamic loading, up to 5 Hz, and high-speed shearing,

Fig. 16 The front view of the Leyte landslide on 17 February 2006. (Taken by K. Sassa from a chartered helicopter. *S* sampling point)
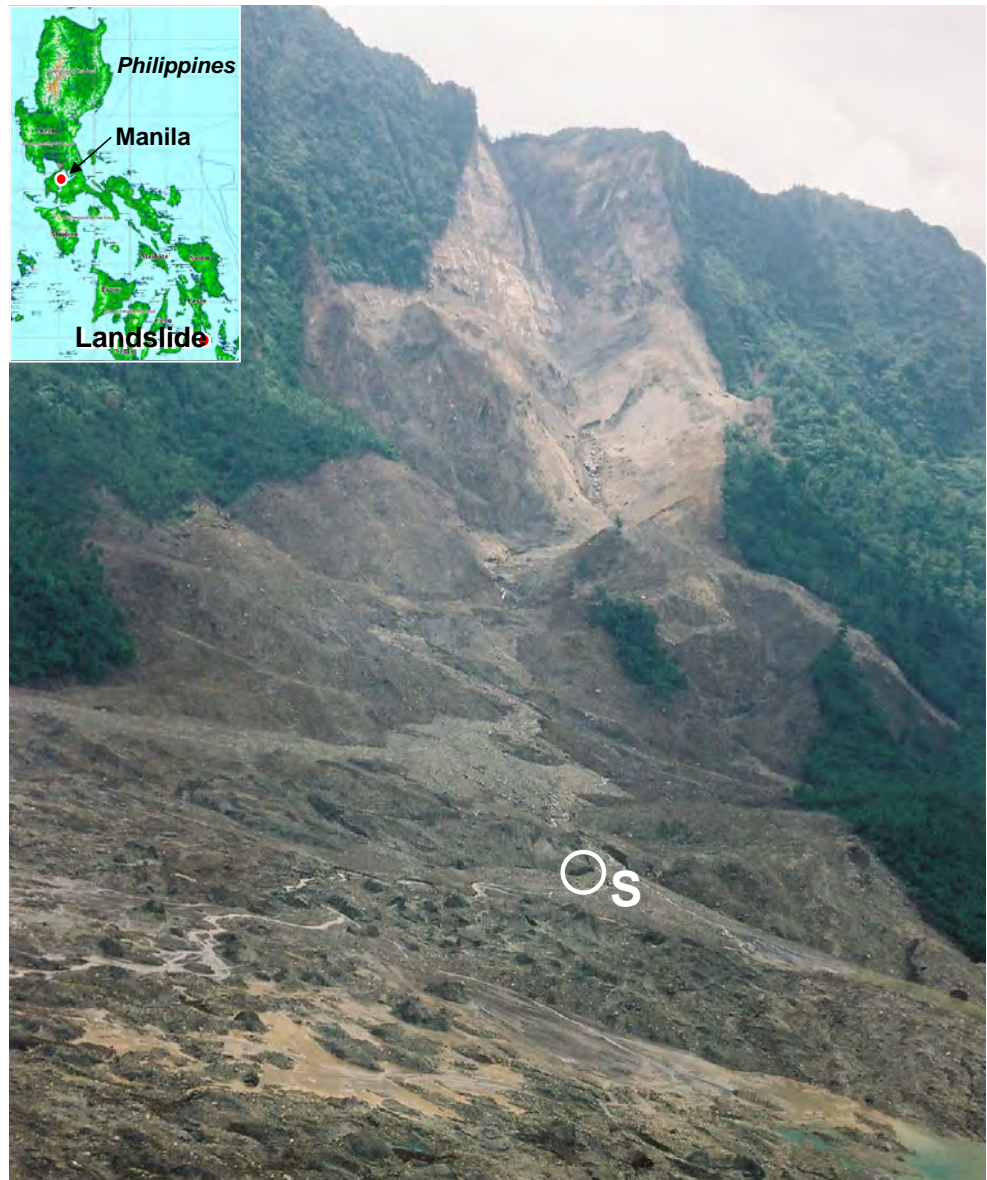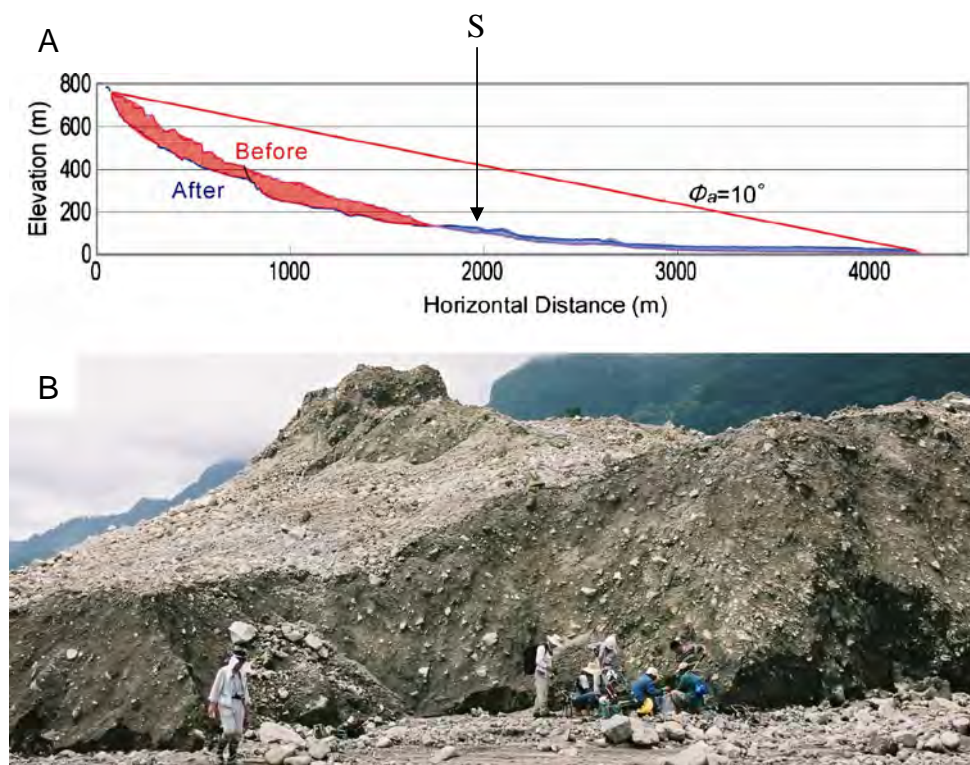
Fig. 17 Field investigation and sampling point S in the Leyte landslide. The location of sampling point is shown as S in Figs. 16 and 17a

up to 224 cm/s. The detail of this apparatus is reported by Sassa et al. 2004a.

The testing procedure of this apparatus is as follows: (1) A sample is taken from the soil layer in which the sliding surface was or will be formed, (2) The sample is set in the ring-shaped shear box, saturated, and consolidated under the stress due to the self-weight of the soil layer, (3) Seismic stress or pore-pressure change due to rainfall are provided, (4) If failure occurs, pore-water pressure and mobilized shear resistance with progress of shear displacement are monitored.

Triggers of landslide

We examined the triggering factors of the Leyte landslide. A small earthquake occurred near the site at the time of occurrence of the landslide, and the location of the hypocenter of this earthquake was estimated by the US Geological Survey (USGS) and the PHIVOLCS. According to PHIVOLCS, the earthquake occurred at a location (10.30 N, 124.90E) 22 km west of the source area of the landslide, 6 km deep, with magnitude Ms 2.6, at 10:36 hours on 17 February 2006. The seismic record at Maasin is shown in Fig. 18. E-W component (blue color) was the major direction of seismic shaking, other two components are around a half magnitude.

Using the standard attenuation function between peak ground acceleration and hypocentral distance (Fukushima & Tanaka 1990), the peak ground acceleration at the landslide site was estimated at 10 gal for this magnitude. We then estimated the expected peak acceleration at the bottom of the landslide mass as about 60–200 gal from the following consideration. (1) Three to five times amplification of ground accelerations at the sliding surface due to the difference in the compression (P) wave speeds between soft volcanoclastic debris (Vp=0.5–1.5 km/s) and hard volcanic bed rock (Vp=2.5–5 km/s) that outcropped in the head

scarp, because the amplification level is proportional to the velocity contrast between two layers. Though the shear (S) wave speeds of the volcanoclastic debris and the bed rock are unclear, similar level of velocity contrast to the P wave is expected at the sediment/bed rock interface. (2) An additional magnification of two to four times is expected in the landslide site due to the focusing of seismic waves onto the mountain ridge. Namely the total magnification of this site will be 6–20 times.

Heavy rainfall (459.2 mm for 3 days on 10–12 February and 571.2 mm for 5 days on 8–12 February 2006) occurred in this area before the day of the landslide as shown in Fig. 18a (PAGASA 2006). This rainfall should have increased the ground-water level and pore-water pressure inside the slope. However, the peak ground-water level had likely depleted before the occurrence of the landslide on 17 February because the rainfall on 13–17 February was small (total 99.0 mm for 5 days). We simulated the ground-water level using a tank model that had been developed to simulate the ground-water level in the Zentoku landslide, Japan (Hong et al. 2005), which had a depth and inclination similar to that of the Leyte landslide. When inputting 10 days' precipitation records at the nearest monitoring station in Otikon (about 7 km west of the landslide) on 8–17 February, the peak ground-water level occurred on 13 February 2006. Because the peak ground-water level had already passed when the landslide occurred on 17 February, we deduced that a small earthquake was the final trigger of the landslide.

Dynamic-loading ring-shear test

Based on this consideration, a dynamic-loading ring-shear test on the sample taken from the landslide was conducted as follows: The sample was set in the shear box (250 mm inside diameter,
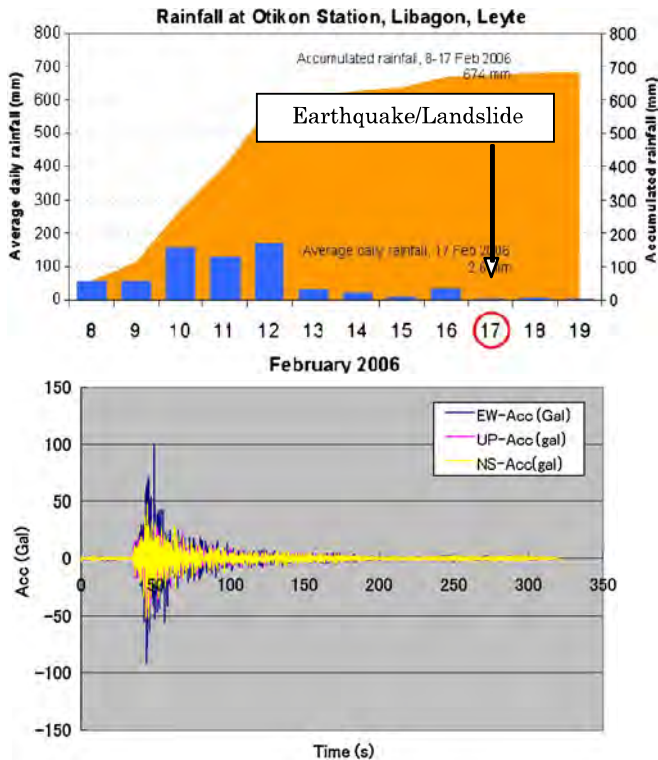
Fig. 18 Triggering factors of the Leyte landslide. Record of rainfalls monitored at Otikon and the earthquake monitored at Maasin, Leyte

350 mm outside diameter) of DPRI-6, and fully saturated ($B_D=$ 0.98). The stress acting on the sliding surface of the deepest part (around 120–200 m) is very high. However, because of the *capacity of this apparatus*: the sliding surface was assumed for the test to be 35 m deep and at an inclination of 25°. The unit weight of the soil was assumed to be 20 kN/m³. In the preliminary test to increase pore-water pressure until failure, the failure line of this material was obtained. It was 39.4° in the friction angle and almost zero cohesion. In the simulation test of a rain- and earthquake-induced landslide, the normal stress corresponding to that of 5 m lower than the critical ground-water level (i.e., further 5 m rise of ground-water level shall trigger the landslide) was first loaded on the sample. Then, the shear stress due to the self-weight of the soil layer was loaded. It is the stress point shown by the white circle in Fig. 19a. Using three components of seismic record observed at Massin (PHIVOLCS, Code number: MSLP, Latitude: 10.1340, Longitude: 124.8590, Elevation: 50.0), normal stress and shear stress acting on the shear surface of 35 m deep with 25° inclination on the direction of the Leyte landslide were calculated so that the peak seismic stress may correspond to the range of seismic acceleration of 60–200 gal, but as low as possible to avoid failure before seismic loading.

Test results
The test results are presented in Fig. 19a–c. Figure 19a presents the stress path of the test. The effective stress path showed a complicate stress path like a cloud. The stress path reached the failure line repeatedly. Therefore, this small seismic stress failed the soil and gave a repeated shear displacement during the period of stress reaching the failure line. It generated a pore water

pressure (blue color line) due to grain crushing and volume reduction, and it was accelerated in progress of shear displacement (green color line). Namely the sliding surface liquefaction phenomenon occurred. The value reached a very small steady-state stress (red color line). This process is presented in the time series data around the failure in Fig. 19b. The mobilized apparent friction coefficient defined by steady-state shear resistance divided by the total normal stress was 0.016 (0.9°). The loaded seismic stress is so small, the control was not easy. The monitored shear resistance is shown in Fig. 19c. When the stress reaches failure line, the balance of shear stress and shear resistance is manifested as acceleration. As seen in the figure, the magnitude of increment of shear resistance seems to be slightly smaller than the decrement. The level of seismic stress is around 40 kPa, the shear stress due to gravity is around 275 kPa. The ratio is 0.145. Namely the seismic coefficient $K=0.145$. The estimated magnitude of stress is to load 60–200 gal, namely $K=0.06$–0.20. This level will be around the filed condition. It was the minimum possible value to avoid failure before seismic loading in some trial test because of stability of initial shear stress loading. This geotechnical simulation test could physically reproduce the rapid landslide motion triggered by a small seismic shaking in a high pore-pressure state due to rain falls. Thus, the combined effect of rainfall and earthquake was confirmed and it should be examined in the new integrated computer simulation.

Computer simulation for the Leyte landslide or a similar landslide

Creating a landslide body
We tried to apply this landslide simulation model to the Leyte landslide or a similar landslide. The digital map of the area is necessary. Though we tried to digitalize the satellite photos (Japanese Satellite, ALOS) using ERDAS Imagine, however, no photo without clouds was obtained. We used the digital map and ground rupture of Southern Leyte Island provided from PHI-VOLCS. However, there is no contour line in the flat area. So contour lines in the flat area were estimated from the measured central line of Fig. 17 and the map edited by the Geographical Survey Institute of Japan (GSI 2006) based on the map made by the National Mapping and Resource Information Agency of Philippines (NAMRIA). The precision of the topography in the flat area may not be always good. The map was made from the air photo taken before the 2006 Leyte landslide. So it did not include the topography of the 2006 Leyte landslide.

We created a landslide body of the 2006 Leyte landslide or a similar landslide by a tool of *LS-RAPID* as an ellipsoid. Quick creation of landslide body is important for practical use. Then, after the various examinations, the following tool was established as shown in Fig. 20. Firstly, we draw the central line of landslide on the map (Fig. 20a) by pointing the top of line and the end of line by a mouse. The section of central section appears in Fig. 20b as a result. Secondly, we will specify two crossing points of the sliding surface and the ground surface as points (A) and (B) by pointing them through the use of a mouse. Thirdly, selecting the location of center of ellipsoid by mouse, a section of ellipsoid appears in Fig. 20b. The location of the center of ellipsoid regulates the angle of sliding surface at the toe of landslide and also at the head scarp.

Then, the location of the crossing point (D) of longitudinal section and crossing section and the elevation value (z) of the center
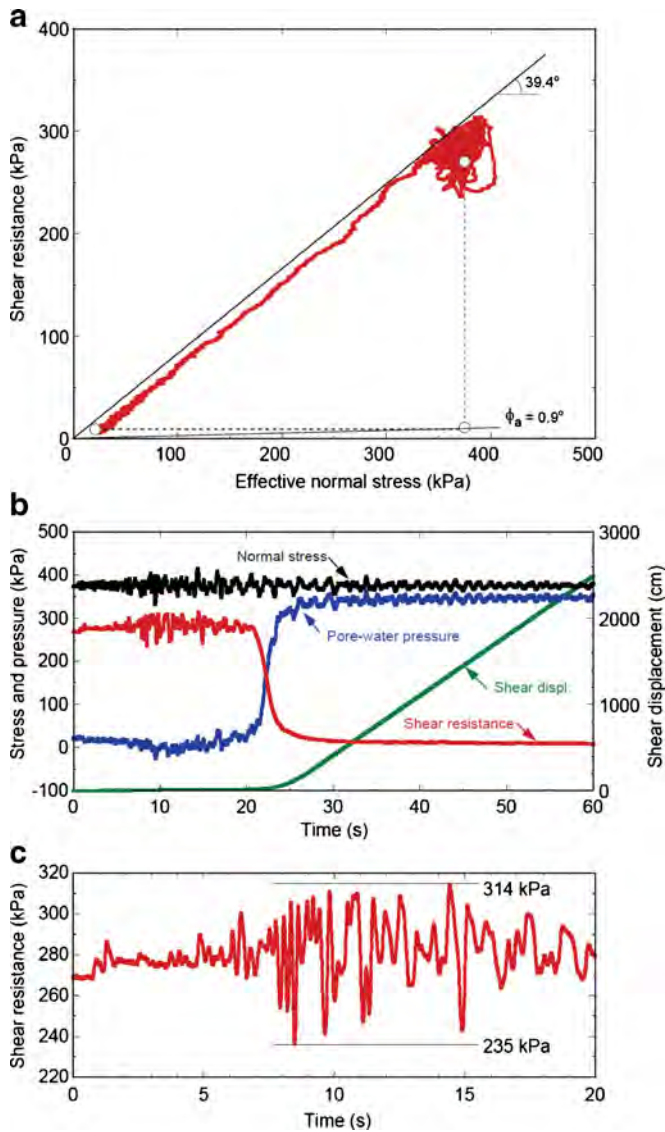
Fig. 19 Undrained seismic loading ring shear test result simulating the 2006 Leyte landslide (B_D=0.98). **a** Stress path; **b** time series data of stresses, pore pressure, shear resistance and shear displacement; **c** enlarged shear resistance monitoring record

of ellipsoid appears in Fig. 20c. Then, we will select one location (x, z) of point C which is located on the ellipsoid line and the x value of Center of ellipsoid by monitoring the shape of landslide body. As a result, the total landslide volume and the vertical maximum depth of landslide are calculated and shown in the box of Fig. 20d. The volume of landslide and the maximum depth are planned to be around 20 million m³ and 120–200 m. The current one of Fig. 20d showed that the volume of created landslide body is 21,038,000 m³, the maximum vertical depth of sliding surface is 188.7 m. Because the real landslide body is not available, this is a simplified landslide body similar to the Leyte landslide.

Conducting simulation

The most important parameter is the steady-state shear resistance (τ_{ss}). The steady-state shear strength is very low as less than 10 kPa in Fig. 19. The testing condition is 100% saturation and the

loading stress corresponding to 35 m deep (much shallower) and the used sample may be more weathered than that in this deep landslide body. So we selected τ_{ss}=40 kPa as a practical value for this landslide. Various combinations of values of factors can be considered. It is not easy, but we assumed the followings: The landslide is deep and the material seems to be intact in the source area as seen in Fig. 16. Then, we estimated that the peak friction and peak cohesion before motion in the source area should be high (tan ϕ_P=0.9, c_P=100–300 kPa); the part of head scarp shown in Fig. 16 would be not saturated because it is close to the ridge, probably there is less ground water to generate excess pore water pressure. Then, B_{ss}=0.1–0.2 was given in this area, and the middle part was probably more saturated (B_{ss}=0.4–0.6) and the lower part in the patty field on the flat area was probably well saturated (B_{ss}=0.9–0.97); The landslide body was stiff in the top, and moderate in the middle and much disturbed in the lower part and on the flat area (lateral pressure ratio k=0.2–0.7); The shear displacement of shear strength reduction was estimated as DL=100 mm, DU=1,000 mm referring to the test of Fig. 19. As for the non-frictional energy consumption, we set threshold values for velocity are 80 m/s in velocity, 200 m in soil height, and energy loss coefficient as α=1.0. As previously explained, almost same results were obtained for α=0.2, 1.0, 2.0, 5.0, and 10.0 in the preliminary tests.

In the trial simulation, no landslide occurred in pore pressure ratio r_u=0.10, 0.15. However, the case of r_u=0.16 caused a rapid landslide. Around 30% saturation in this source area is the critical value to trigger a landslide without earthquake. Then, various magnitude of seismic shaking using the wave forms of EW, NS, and UD recorded at Maasin, Leyte were given in addition to pore pressure ratio of 0.15. The border to create a rapid landslide existed between K_{EW}=0.11 and 0.12. Then, we gave K_{EW}=0.12. Using the ratio of magnitudes of seismic records of EW, NS and UD, K_{NS}=K_{UD}= 0.061. The seismic shaking of three directions of EW, NS and UD were given in this simulation. 3 m unstable deposits are assumed in the alluvial deposit area. Blue balls shown in Fig. 21a are the unstable soil deposits (initial landslide body) in the source area and also unstable deposits in the alluvial flat area. The critical height (Δh_{cr}=0.5 m) to reduce shear strength from peak to the steady state was given. The threshold values that trigger the function for non-frictional energy consumption are 200 m in the soil height and 80 m/s in velocity.

200 m was set to be a bit greater than the maximum depth of the initial landslide body (188.7 m) because the height will decrease after the start of motion; 80 m was decided to be around 3–4 times greater than the velocity of 20–26 m/s observed in the 1984 Ontake rapid landslide in volcanoclastic debris which was a greater 3.6×10⁷ m³ in volume and traveled over 9 km.

A series of motion with explanation for each step was presented in the case of K_{EW}=0.12, K_{NS}=K_{UD}=0.061, r_u=0.15 in Fig. 21. The air photo taken from the helicopter and the simulation results presented in 3D view from a similar angle are presented in Fig. 22. The travel distance and the major part of landslide distribution were well reproduced. The secondary debris flow and muddy water spread to the leftward in the photo and field observation. These are not presented in the computer simulation.

Conclusions

1. A new computer simulation model (*LS-RAPID*) was developed. It integrated the *stability analysis* from a stable state to
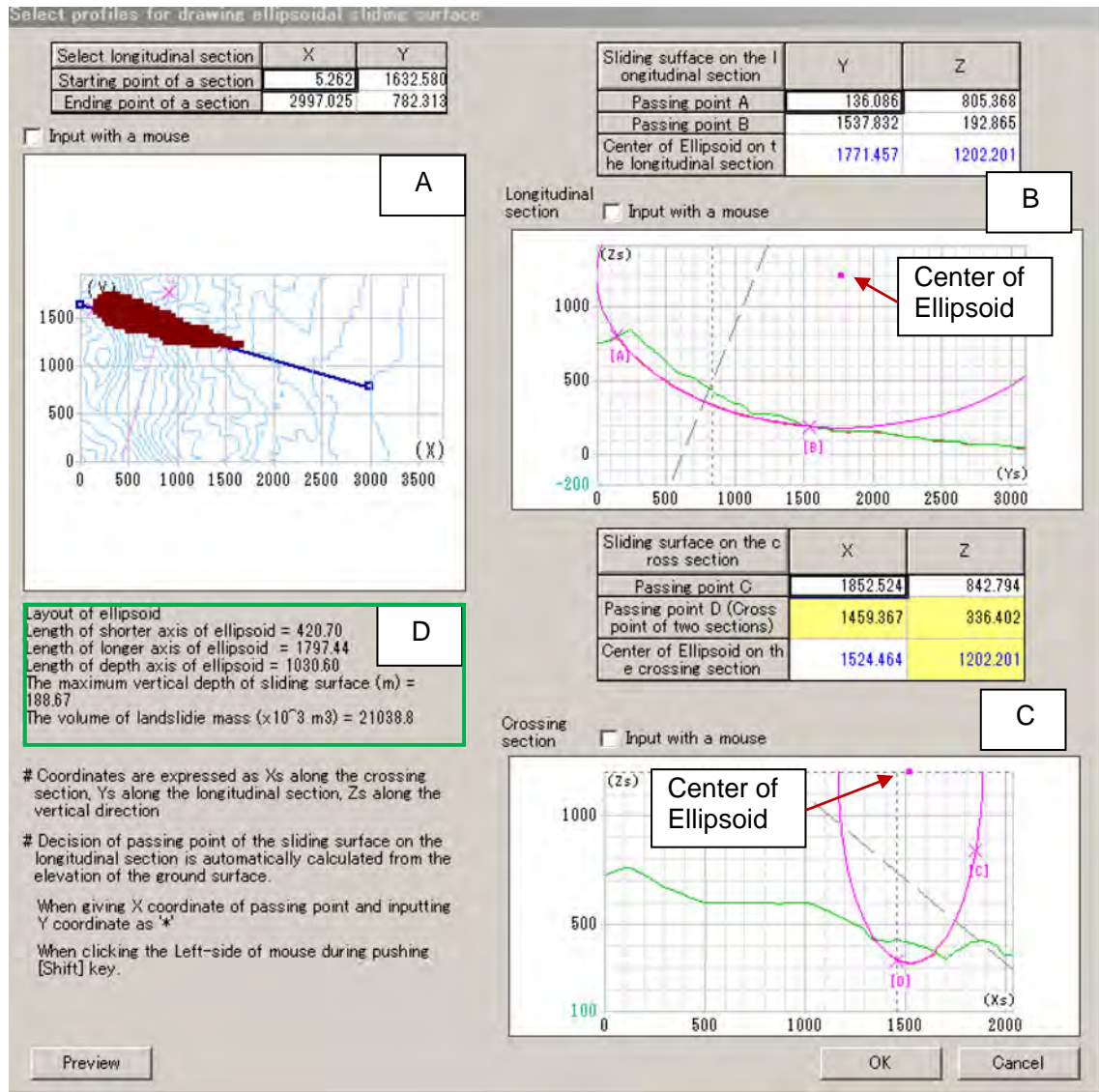
Fig. 20 Creating a landslide body as an ellipsoid. **a** The central line is selected in the plan map. **b** Two crossing points of the sliding surface to the ground surface and the center of ellipsoid are selected. **c** Another point (*C*) on the ellipsoid line and *x*-axis value of the center of ellipsoid are selected. **d** Volume, depth, and others of the landslide body are shown

the failure (initiation of landslide) triggered by pore pressure increase and/or seismic loading, and the *dynamic analysis* for the post-failure motion. The reduction of shear resistance from the peak to the stead state was modeled and incorporated in this program.

2. The computer program could reproduce the progressive failure of the slope because shear resistance starts to decrease where/when the shear displacement reaches the threshold value of shear displacement.

3. Comparison of *LS-RAPID* and conventional limit equilibrium stability analyses of Bishop, Janbu, Spensor, Morgenstern and Price showed that landslides will be initiated in smaller power water pressure ratio in *LS-RAPID* because of progressive failure. The threshold value of start of shear strength reduction was changed from 10 mm (estimated from experiments) to 2,000 mm (a large value) to restraint the initiation of progressive failure. In this case, the border between motion

and no motion in *LS-RAPID* was the same with the border by conventional limit equilibrium stability analyses.

4. The new computer simulation was applied to the 2006 Leyte landslide based on the values measured in laboratory and monitored seismic records. Key parameter of the steady-state shear resistance was decided based on the result of laboratory test though it was not complete because the loaded normal stress is different due to the limited capability of the apparatus. The computer simulation reproduced a rapid landslide with a similar travel distance and distribution area which was triggered by a pore water pressure ratio of 0.15 and a small seismic shaking of $K_{EW}=0.12$ and K_{NS} and $K_{UD}=0.061$ using the seismic wave forms recorded at the Maasin observatory. The simulation result almost corresponded that the rapid landslide triggered by a small nearby earthquake of $Ms=2.6$ in 5 days after the consecutives heavy rains for 3 days intensity of over 100 mm/day.
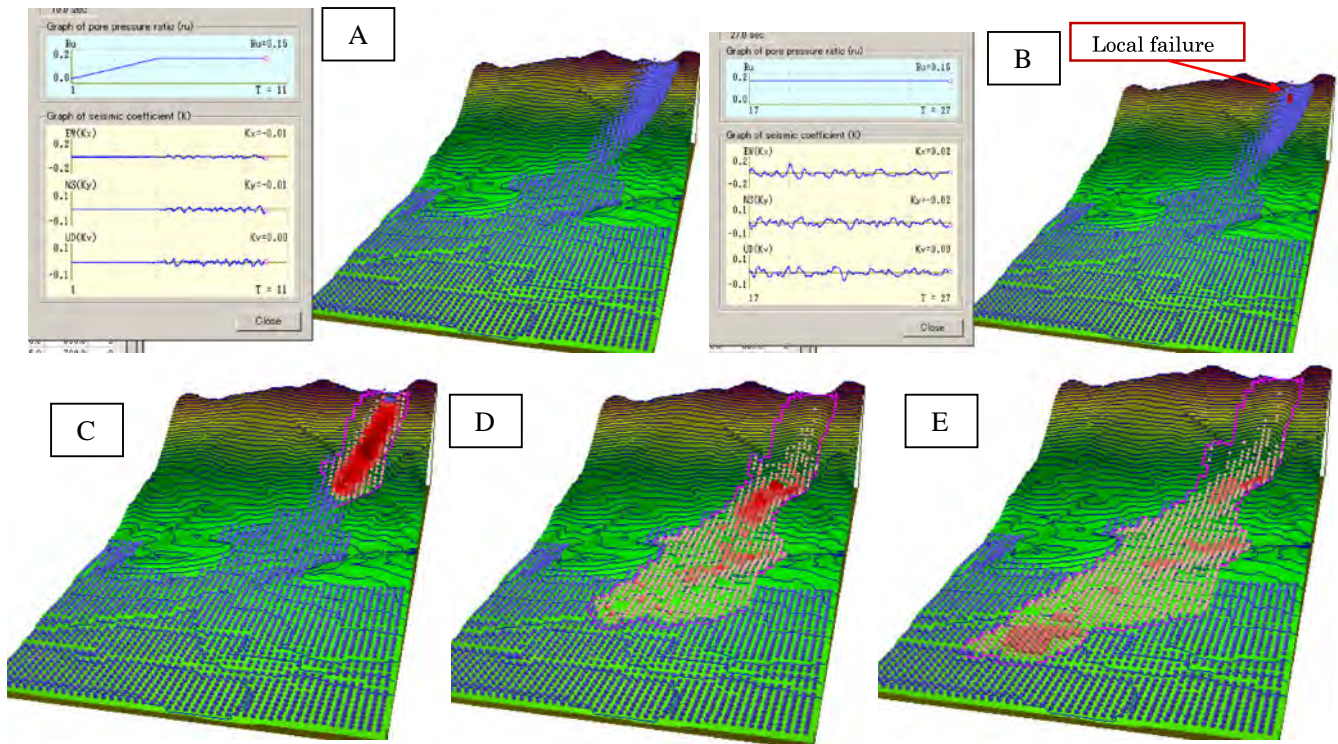
Fig. 21 Simulation result of the Leyte landslide. **a** r_u rises to 0.15 and earthquake will start but no motion. **b** Continued earthquake loading (Max $K_{(EW)}=0.12$, $K_{NS}=K_{UD}=0.061$) triggers a local failure as presented in red color mesh, **c** an entire landslide block is formed and moving, **d** the top of landslide mass goes on to alluvial deposits, **e** deposition. Mesh, 40 m; Area, 1,960×3,760 m; contour line, 20 m; 3 m unstable deposits in the alluvial deposit area (*blue balls*)

5. We made efforts to design this computer simulation run by note personal computer in a user friendly way. All simulations of this paper was conducted by a notebook personal computer (Sony VAIO VPCZ1, 64 bit, core i7, 2.67 GHz, memory 8.00 GB).

6. Profiles of sections, values of triggering factors, the values of depth distribution, velocity distribution and mobilized apparent friction (calculated from the steady-state shear resistance and the soil depth) at different site/time can be monitored during motion. Video and photos of motion can be recorded.

Those are useful for analysis of the moving process and performance of simulation and further improvement through the application for various case studies.
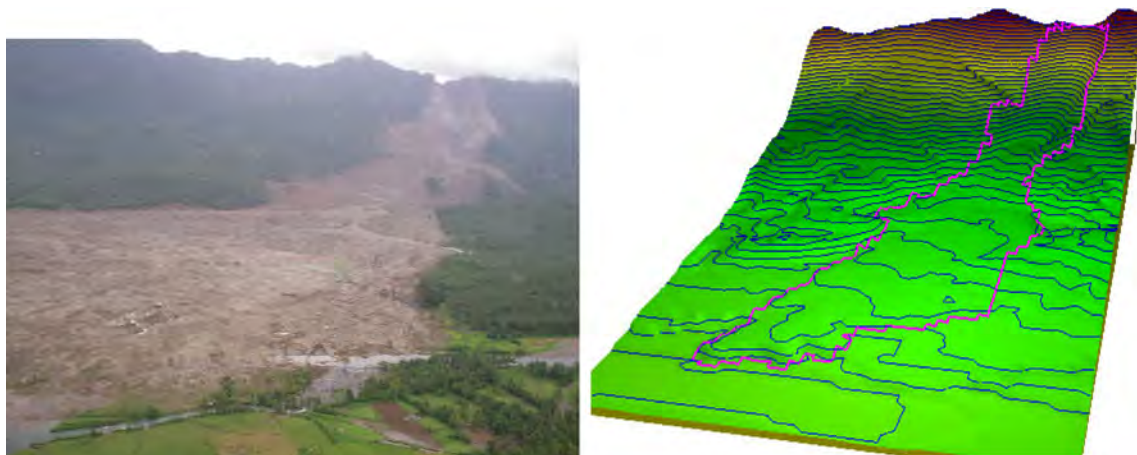
Fig. 22 Air photo and the result of computer simulation of the Leyte landslide. Air photo taken from the chartered helicopter by a member of Japan–Philippines investigation team (K. Araiba). The travel distance and the major part of landslide distribution were well reproduced. The secondary debris flow and muddy water spreads to the leftward in the photo and field observation. Those are not presented in the computer simulation@

References

Araiba K, Nagura H, Jeong B, Koarai M, Sato H, Osanai N, Itoh H, Sassa K (2008) Topography of failed and deposited areas of the large collapse in Southern Leyte, Philippines occurred on 17 February 2006. In: Proc. International Conference on Management of Landslide Hazard in the Asia-Pacific Region (Satellite Symposium on the First World Landslide Forum). pp 434–443

Catane SG, Cabria HB, Tomarong CP, Saturay RM, Zarco MA, Pioquinto WC (2007) Catastrophic rockslide-debris avalanche at St. Bernard, Southern Leyte, Philippines. Landslides 4(1):85–90

Chen H, Lee CF (2003) A dynamic mode for rainfall-induced landslides on natural slopes. Geomorphology 51:269–288

Chen H, Lee CF (2007) Landslide mobility analysis using MADFLOW. Proc The 2007 International Forum on Landslide Disaster Management 2:857–874

Denlinger RP, Iverson RM (2004) Granular avalanches across irregular three-dimensional terrain: 1. Theory and computation. J Geophys Res 106(F01014):14

Fukushima Y, Tanaka T (1990) A new attenuation relation for peak horizontal acceleration of strong earthquake ground motion in Japan. Bull Seismol Soc Am 84:757–783

GSI (2006) 1:50,000 topographical map "Surroundding area of Leyte landslide", Geological Survey Institute of Japan

Hong Y, Hiura H, Shino K, Sassa K, Fukuoka H (2005) Quantitative assessment on the influence of heavy rainfall on the crystalline schist aldnslide by monitoirng system—case study on Zentoku landslide in Japan. Landslides 2-1:31–41

Hungr O (2009) Numerical modelling of the motion of rapid, flow-like landslides for hazard assessment. KSCE J Civ Eng 13(4):281–287

Hungr O, KcKinnon M, McDougall S.(2007a). Two models for analysis of landslide motion: Application to the 2007 Hong Kong benchmarking exersies. In: Proc. the 2007 International Forum on landslide disaster management, vol. 2. pp 919–932

Hungr O, Morgenstern NR, Wong HN (2007b). Review of benchmarking exercise on landslide debris runout and mobility modelling. In: Proc. the 2007 International Forum on landslide disaster management, vol. 2. pp 755–812

Igwe O, Sassa K, Wang FW (2007) The influence of grading on the shear strength of loose sands in stress-controlled ring shear tests. Landslides 4(1):43–51

Körner, H (1980). Model conceptions for the rock slide and avalanche movement. Proc. Iternational Symposium "INTERPRAEVENT 1980", Bad Ischl, vol. 2. pp 15–55

Kwan J, Sun HW (2007). Benchmarking exercise on landslide mobility modelling-runout anayses using 3dDMM. In: Proc. the 2007 International Forum on landslide disaster management, vol.2. pp 945–966

Okada Y, Sassa K, Fukuoka H (2000) Liquefaction and the steady state of weathered granite sands obtained by undrained ring shear tests: a fundamental study on the mechanism of liquidized landslides. J Nat Disaster Sci 22(2):75–85

Philippine Atmospheric, Geophysical and Astronomical Services Agency (PAGASA) (2006) Precipitation record at Otikon, Libagon

PHIVOLCS (2008) Digital map and ground rupture of Southern Leyte Island. Philippine Institute of Volcanology and Seismology (PHIVOLCS) in CD

Sassa K (1988) Geotechnical model for the motion of landslides. In: Proc. 5th International Symposium on Landslides, "Landslides", Balkema, Rotterdam, vol. 1. pp 37–56

Sassa K, Fukuoka H, Wang G, Ishikawa N (2004a) Undrained dynamic-loading ring-shear apparatus and its application to landslide dynamics. Landslides 1(1):7–19

Sassa K, Wang G, Fukuoka H, Wang FW, Ochiai T, Sugiyama, Sekiguchi T (2004b) Landslide risk evaluation and hazard mapping for rapid and long-travel landslides in urban development areas. Landslides 1(3):221–235

Sassa K, Fukuoka H, Wang FW, Wang GH (2007) Landslides induced by a combined effects of earthquake and rainfall. Progress in Landslide Science (Editors: Sassa , Fukuoka, Wang, Wang), Springer, Berlin. pp 311–325

Sassa K, Fukuoka H, Solidum R, Wang G, Marui H, Furumura T, Wang F (2008) Mechanism of the initiation and motion of the 2006 Leyte landslide, Philippines. In: Proc International Conference-Workshop "Guinsaugon 2008—Living with Landslides (in CD)

Stone R (2009) Peril in the Pamirs. Science 326:1614–1617

Takahashi T, Tsujimoto H (2000) A mechanical model for Merapi-type pyroclastic flow. J Volcanol Geotherm Res 98:91–115

Wang FW, Sassa K (2007). Landslide simulation by geotechnical model adopting a model for variable apparent friction coefficient. In: Proc. the 2007 International Forum on landslide disaster management, vol. 2. pp 1079–1096

Zhang D, Sassa K (1996) A study of the apparent friction angle after failure during undrained shear of loess soils. J Japan Soc Erosion Control Eng 49(3):20–27

K. Sassa (✉) · **O. Nagai**
International Consortium on Landslides,
Kyoto, Japan
e-mail: sassa@iclhq.org
e-mail: nagai@iclhq.org

R. Solidum
Philippine Institute of Volcanology and Seismology (PHIVOLCS),
Quezon City, Philippines
e-mail: solidr@phivolcs.dost.gov.ph

Y. Yamazaki
GODAI Development Corporation,
Kanazawa, Japan
e-mail: yamazaki@godai.co.jp

H. Ohta
Ohta Geo-Research Co., Ltd.,
Nishinomiya, Japan
e-mail: ohta@ohta-geo.co.jp